THE JOURNAL OF PHYSICAL CHEMISTRY C

Article

pubs.acs.org/JPCC

Overgrowth of Rhodium on Gold Nanorods

Ruth L. Chantry,[†] Wilai Siriwatcharapiboon,[‡] Sarah L. Horswell,*[,‡] Andrew J. Logsdail,[‡] Roy L. Johnston,[‡] and Z. Y. Li*[,†]

[†]Nanoscale Physics Research Laboratory, School of Physics and Astronomy, [‡]School of Chemistry, University of Birmingham, Edgbaston, Birmingham, B15 2TT, United Kingdom

ABSTRACT: This study focuses on the deposition and growth mode of rhodium (Rh) on gold (Au) seed nanorods (NRs). Using a combination of scanning transmission electron microscopy imaging, energy-dispersive X-ray spectroscopy, and UV−visible absorption spectroscopy, we show that Rh deposition results in an uneven overlayer morphology on the Au NR seeds, with a tendency for Rh deposition to occur preferentially on the Au NR ends. The results suggest that complex and kinetically driven metal−metal interactions take place in this system.

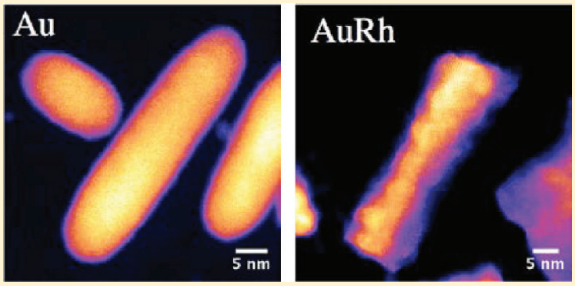

INTRODUCTION

There has been considerable interest in nanoparticles in recent years as a result of the advances made in their synthesis and the identification of many potential applications for which they may be suited.[1] The properties of nanoparticles vary considerably with both size and structure, which, in principle, allows the potential to tune their properties to specific requirements.[2,3] For bimetallic nanoparticles, properties also vary with composition and chemical ordering, affording yet further opportunities for tuning properties through manipulation of the interaction between their constituent metals.[4] The effective exploitation of bimetallic nanoparticles will depend on fully characterizing their structure and understanding how the interactions between their constituent metals impact their properties.

In this study we focus on the deposition and growth mode of Rh on Au seed nanorods (NRs). While Rh is catalytically active in bulk form, Au has only been found to demonstrate catalytic activity in nanoscale systems.[5] Au nanoparticles have tunable surface plasmon responses at visible wavelengths, whereas the surface plasmon of Rh occurs in the UV range and has not been well characterized in nanoparticles. The energetic and structural characteristics of these metals also make the AuRh NR system of interest: the 7% lattice mismatch (Au 0.408 nm vs Rh 0.380 nm)[6] and higher bulk cohesive energy (Au 3.8 eV/atom vs Rh 5.8 eV/atom)[6] and surface energy (Au 1.6 J/m^2 vs Rh 2.8 J/m^2)[7] of Rh compared with Au mean that a system of Rh sequentially deposited onto Au may not be in thermodynamic equilibrium, potentially leading to interesting behavior and associated properties at the nanoscale. Despite the interesting and contrasting physical and chemical properties of these two elements, there are limited reports in the literature concerning the experimental investigation of AuRh nanostructured systems. Core−shell structures have been studied using surface science techniques on samples synthesized by physical vapor deposition, reporting a tendency for Au coverage of Rh on TiO_2 substrates when Rh is deposited first and for Rh migration to subsurface sites when Au is deposited first.[7,8] This behavior is in accordance with their relative surface energies. With regard to the colloidal chemical synthesis of AuRh systems, only one report has been made, where coreduction was found to result in alloyed AuRh nanoparticles.[9] Here we report, for the first time, that $Au_{core}Rh_{shell}$ NRs can be chemically synthesized and that the resulting core−shell structure is stable under ambient conditions over a prolonged period, providing direct evidence of their structure through atomically resolved scanning transmission electron microscopy (STEM) imaging, supported by analysis of their surface plasmon absorption and energy-dispersive X-ray spectroscopy (EDX). We further identify the initial Rh deposition occurring at rod ends and corners. The structural stability of this system is discussed based on thermodynamic considerations.

EXPERIMENTAL METHODS

Chemicals and Reagents. All reagents used were analytical grade or better and were used as received. Cetyltrimethylammonium bromide (CTAB) and L-ascorbic acid were purchased from Acros, whereas sodium borohydride ($NaBH_4$) was obtained from Riedel-de Haën and silver nitrate ($AgNO_3$) was from Sigma Aldrich. Hydrogen tetrachloroauric acid ($HAuCl_4 \cdot 3H_2O$) and sodium hexachlororhodate ($Na_3RhCl_6 \cdot 12H_2O$), both premium grade, were purchased from Alfa Aesar. Ultrapure water (purified with a Milli-Q tandem Elix-Gradient A10 system: resistivity 18.2 MΩ cm, TOC ≤ 5 ppb) was used throughout. All glassware used was first cleaned by heating in a mixture of concentrated nitric and sulfuric acids for 1.5 h, followed by rinsing with copious quantities of ultrapure water and soaking overnight in ultrapure water.

Received: December 23, 2011
Revised: March 31, 2012
Published: April 16, 2012

ACS Publications © 2012 American Chemical Society

dx.doi.org/10.1021/jp212432g | J. Phys. Chem. C 2012, 116, 10312−10317

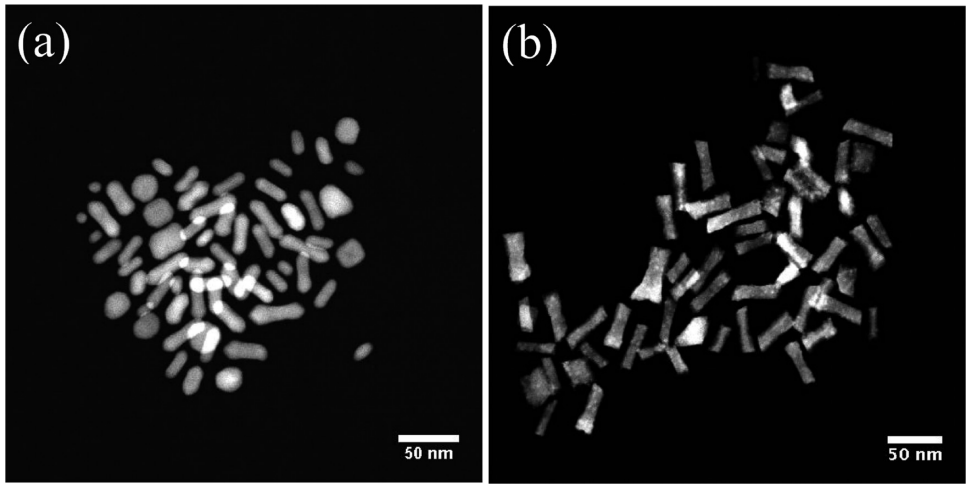

Figure 1. Representative STEM-HAADF images of (a) Au seed and (b) $Au_{core}Rh_{shell}$ nanorods.

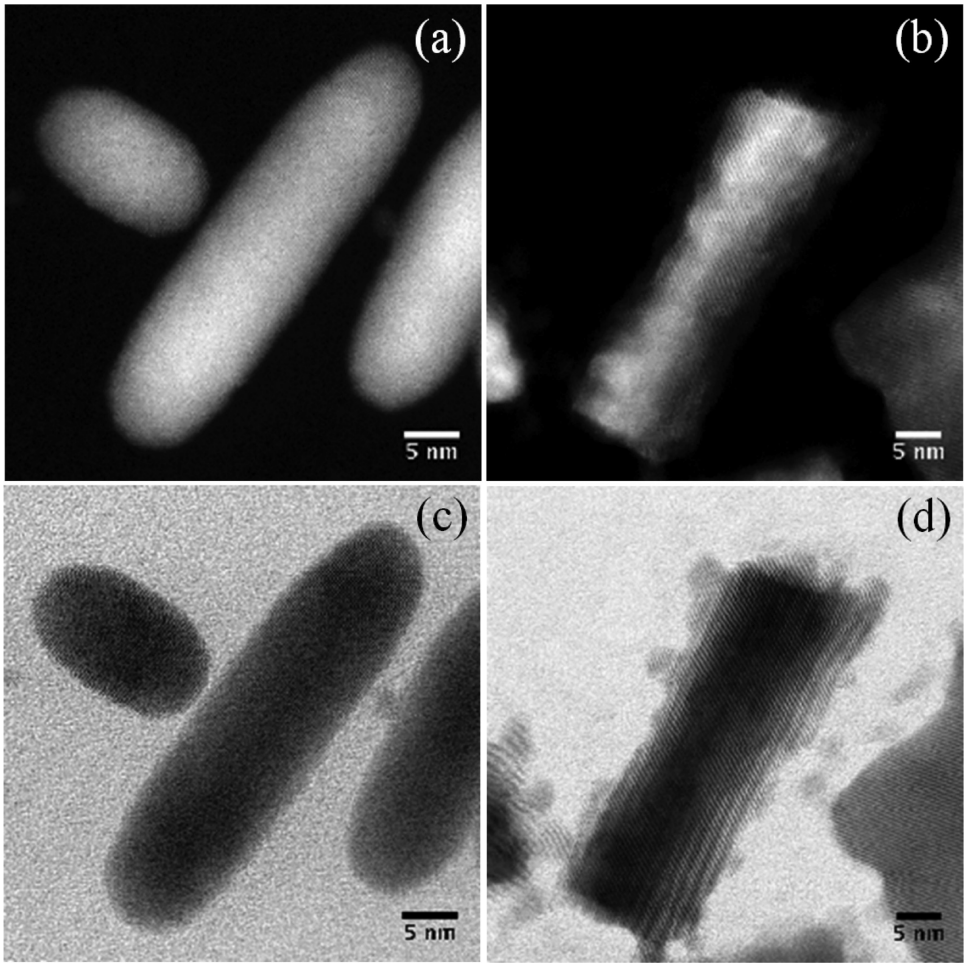

Figure 2. STEM-HAADF images of typical examples of (a) Au seed nanorod and (b) $Au_{core}Rh_{shell}$ nanorod, together with their corresponding simultaneously acquired STEM-BF images, (c) and (d).

Sample Preparation. The AuRh NRs were synthesized using a seed-mediated sequential growth method. The Au seed NRs were synthesized using the method of Nikoobakht et al.,[10] as modified by He et al.[11] This method involves the use of $AgNO_3$ to promote shape and aspect ratio control during Au NR growth.[12] Rh was deposited onto the Au NRs by reducing a 0.002 M aqueous solution of sodium hexachlororhodate on to the Au NRs. 6 mL Au NR solution was centrifuged at 6000 rpm for 1 h to remove excess CTAB and nanospheres. The supernatant was removed using a pipet, and the NRs were redispersed in 0.5 mL of ultrapure water. The molar ratio of Au:Rh was varied by mixing 0.5 mL Au NR solution with different volumes of 0.002 M $Na_3RhCl_6{\cdot}12H_2O$ reagent (0.15, 0.643, 1.5, and 3.0 mL), giving samples with molar ratios Au:Rh

dx.doi.org/10.1021/jp212432g | J. Phys. Chem. C 2012, 116, 10312–10317

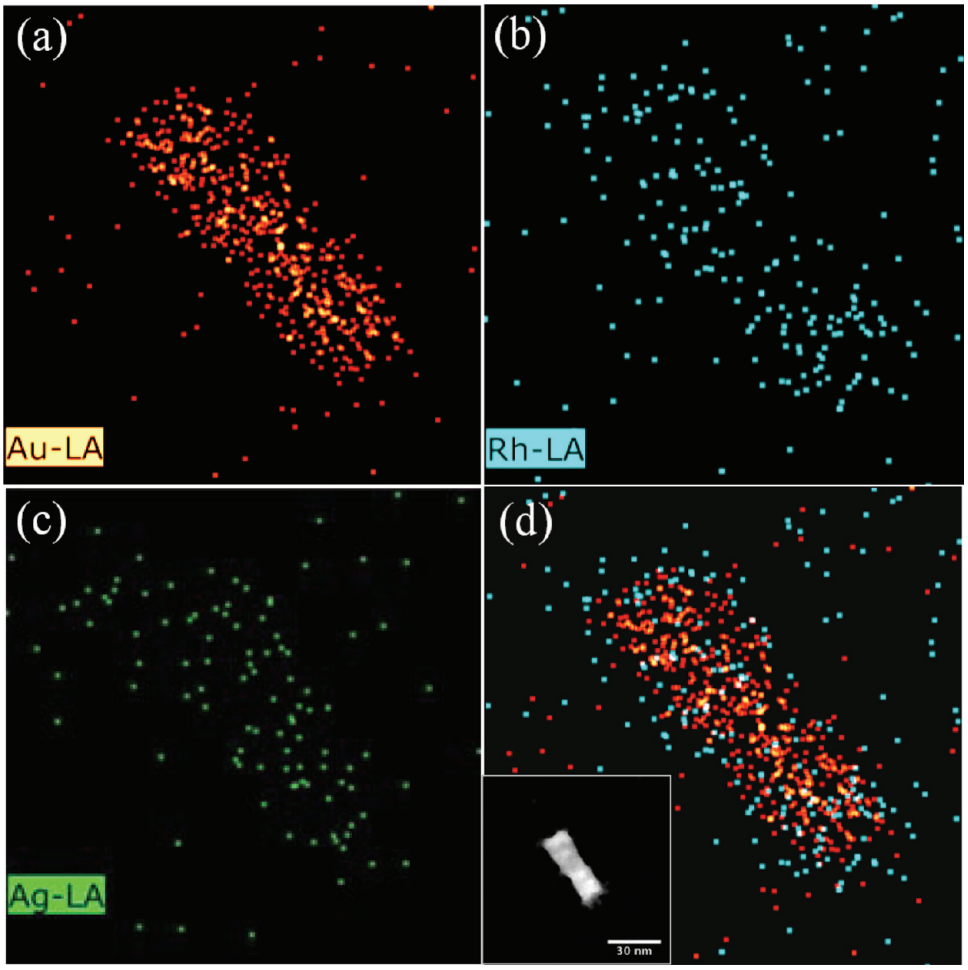

Figure 3. EDX maps of (a) Au, (b) Rh, and (c) Ag, with (d) an overlay of panels a and b, showing the relative locations of the Au and Rh signals, with corresponding STEM-HAADF image inset.

of 10:1, 7:3, 1:1, and 1:2. 1 mL of 0.2 M ascorbic acid was added, and the total volume of each sample was adjusted to 4.5 mL. The mixture was stirred for 2 h at 40 °C.

Characterization Techniques. STEM imaging was carried out using a Jeol 2100F STEM, fitted with a CEOS spherical aberration corrector and a high-angle annular dark field (HAADF) detector, operated at an accelerating voltage of 200 kV. The microscope is also equipped with a Bruker XFlash 4030 SDD detector enabling EDX measurements. The samples were drop-cast in aqueous solution onto amorphous carbon-coated copper grids and left to dry under ambient conditions for at least 24 h prior to imaging. Scanning electron microscopy (SEM) imaging was performed using an FEI SFEG30 operated at 10 kV. A Camspec M550 double-beam spectrophotometer was employed for UV−vis absorption measurements, and the optical response of the NRs was simulated using the DDSCAT program.[13]

■ RESULTS AND DISCUSSION

Figure 1 shows overview STEM-HAADF images of Au NRs before and after Rh deposition. The successful deposition of Rh onto the Au seed NRs is evident in the comparison between the smooth, rounded appearance of the bare Au NRs and the uneven and angular appearance of the AuRh NRs. Representative high-resolution STEM-HAADF images of both types of NRs are shown in Figure 2a,b, respectively, together with simultaneously acquired STEM bright-field (STEM-BF) images in Figure 2c,d. For a system of Rh on Au, the distinct difference in the atomic numbers of two elements (45 and 79, respectively) enables us to attribute the variation in HAADF contrast in Figure 2b, between the center of the NR and the outer edges of the NR, to core/shell structure,[14−16] consistent with the sequential synthesis method followed. Figure 2d shows the full extent of Rh overgrowth that is not apparent in the HAADF image of Figure 2b due to the low contrast at the rod edges. The uneven morphology shown indicates an island growth mode of Rh on Au NRs.

EDX measurements have been conducted on the AuRh NRs. Figure 3a−c displays elemental maps of Au, Rh, and Ag, respectively. Figure 3d shows the relative location of Au and Rh, and the inset is the corresponding STEM-HAADF image taken from the same rod. Despite the limited spatial resolution of the EDX detector used, the clear correlation in the pattern of Au and Rh signals supports the core−shell structure discussed above. The Ag residue left from the synthesis of Au NRs may cause a rod-end preference deposition for Rh, as has been previously suggested for Pt on Au rods.[17]

Further evidence of the Rh deposition on Au NR seeds was found in UV−vis absorption measurements, as shown in Figure 4a. The intense feature at 755 nm for the Au-only seed rod can be attributed to the longitudinal surface plasmon (LSP) resonance.[18] A progressive damping of response and red shift

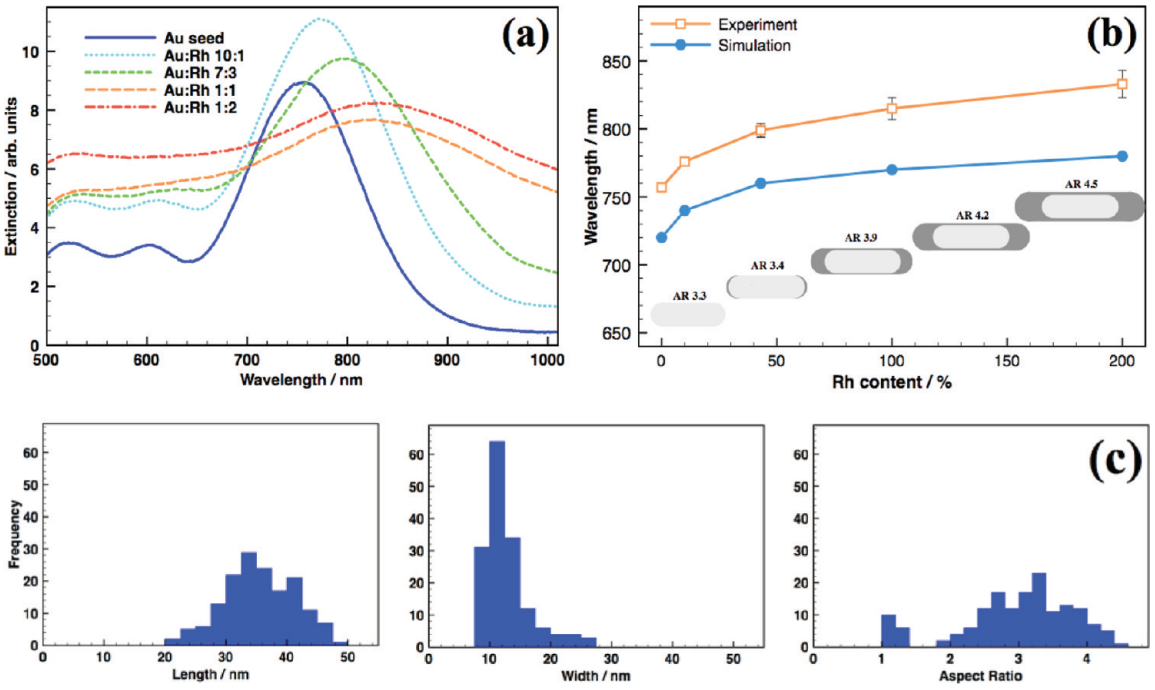

Figure 4. (a) UV−visible spectra of Au seed and $Au_{core}Rh_{shell}$ 10:1, 7:3, 1:1, and 1:2 nanorods, (b) comparison of the longitudinal surface plasmon peak position from the UV−vis experiment and DDA simulation across a range of Rh content from 0 to 200%, and (c) histograms of length, width, and aspect ratio of Au seed nanorods (measured from scanning electron microscope images not shown here).

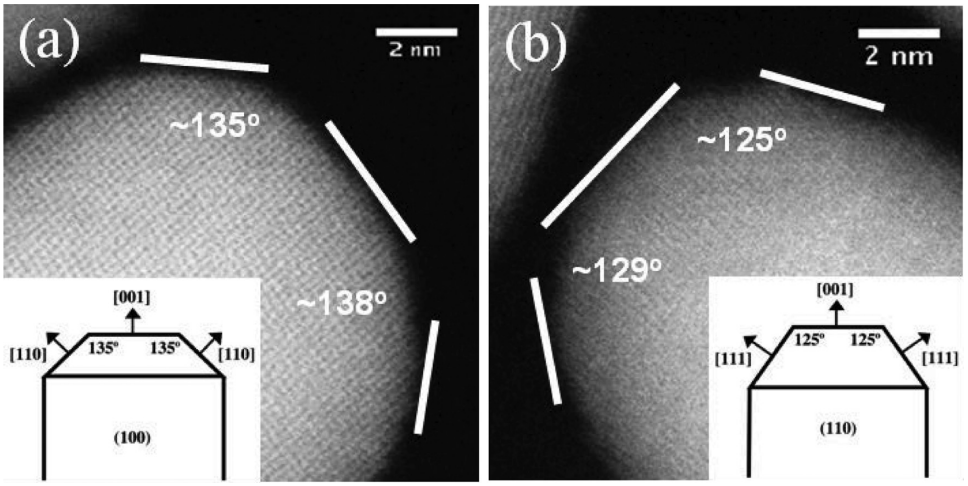

Figure 5. STEM-HAADF images of two Au nanorods, (a) a more rounded end and (b) a less rounded end.

of the peak from 755 to 830 nm for increasing Au:Rh molar ratios is suggestive of successful sequential deposition of Rh.

To establish the link between STEM imaging of these AuRh samples with their surface plasmon results, we performed simulations of their optical response, using the discrete dipole approximation (DDA), using DDSCAT software,[13] with custom-made shapes based on dimensions measured from SEM images of Au seed NRs. For simulation, the Rh shell was treated as evenly coating the Au seed rod core; this is consistent with the ensemble nature of UV−vis results but, as is clear from Figure 2b, is not accurate in respect of individual NRs. Schematics representative of the custom shapes used for DDSCAT simulation are shown in Figure 4b, and the Au seed NR size analysis on which these were based is given in Figure 4c. Figure 4b shows a comparison of experimental LSP wavelengths with the simulations for the different atomic composition of Au:Rh across the samples. Although the simulation consistently slightly underestimates the surface plasmon wavelength, the trend of peak red shift with increasing Rh content is well matched between simulation and experimental results, suggesting that the red shift can be attributed to the increasing aspect ratio in NRs caused by the preferential Rh deposition at the rod ends.

To gain insight into the Rh growth mechanism, we performed detailed characterization of Au NRs at the atomic scale. Figure 5a,b shows two typical images of Au rod ends with more rounded and less rounded morphologies, respectively. The angles between rod end facets are found to have values consistent with the facet structure schematics shown in the insets. Wang et al. proposed a single-crystal model for the structure of Au NRs consisting of a rod end terminated by a (001) face, connected to the body of the rod by alternating

dx.doi.org/10.1021/jp212432g | J. Phys. Chem. C 2012, 116, 10312−10317

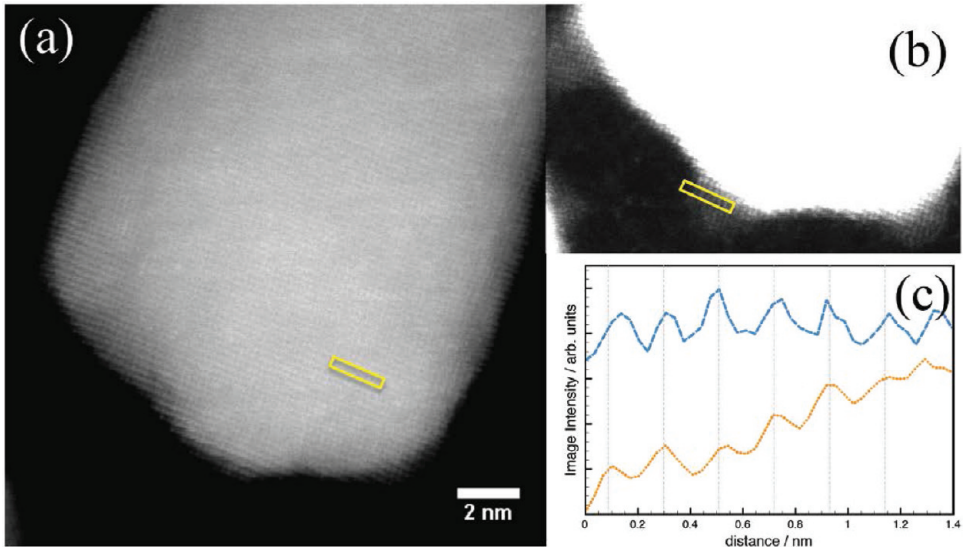

Figure 6. STEM-HAADF images of (a) the end of a AuRh rod with low Rh coverage and (b) high contrast extract from panel a. (c) Intensity profiles taken from as marked in panels a and b with, respectively, blue dashed and orange dotted lines.

{110} and {111} facets. The body comprises alternating {100} and {110} facets.[19] An alternative model for single-crystal Au NRs, comprising end pyramids of {013} facets, and {0 5 12} side and end linking facets has recently been proposed.[20] However, the structures and facet angle measurements illustrated in Figure 5a,b indicate that the Au seed NRs used in this study have a facet structure consistent with the Wang et al. model.

Figure 6a is a high-resolution STEM-HAADF image of the end part of a AuRh rod with low atomic composition of Rh/Au; a high contrast extract from this image given in Figure 6b reveals outgrowths of Rh that may have occurred specific to certain end and corner facets of the Au NR. The line profiles shown in Figure 6c were taken from the regions indicated in panels a and b, with intensity taken over a width of 0.20 nm. It shows a good lattice match between the body of the rod and the Rh outgrowth, with a mean spacing of 0.20 ± 0.01 nm for both over the regions indicated, which is consistent with the [002] lattice spacing of Au.[6] Studies by Kibler et al., using scanning tunneling microscopy, found that Rh deposited on Au followed an island growth mode after the initial formation of a bilayer.[21] The outgrowths apparent in Figure 6b appear to be consistent with the island growth mode. It is likely that the initial preference for Rh deposition on the end facets of the Au NRs, together with the formation of Rh outgrowths from the rod, persists through thicker Rh deposition, as shown in Figure 2b, resulting in an increase in aspect ratio and the observed red shift in longitudinal plasmon response shown in Figure 4.

The complex growth mode identified by this study is consistent with the large lattice mismatch strain (~7%) between Au and Rh and also with the lack of thermodynamic equilibrium in this system. Both the higher surface energy of Rh and the smaller lattice constant of Rh favor Au coverage of Rh, and this behavior has been found in AuRh systems on TiO_2, formed by sequential deposition of Rh and then Au, resulting in a $Rh_{core}Au_{shell}$ structure.[8] Similar behavior has also been found in a system of $Pt_{core}Au_{shell}$ nanoparticles on a TiO_2 support, consistent with their relative surface energies.[22] In contrast with these studies, the work presented here has revealed the successful deposition of Rh on to Au seeds to produce $Au_{core}Rh_{shell}$ NRs. Possible explanations for this difference include the role played by the TiO_2 substrate and the temperature during physical vapor deposition in previous studies[8] or, alternatively, the ligands used in the chemical synthesis method followed for the samples studied here may play a part in stabilizing the core–shell structure. The uneven morphology of Rh on Au found in this study may suggest that the growth progressed at different rates dependent on the atomic facets.

These NRs show no clear sign of degrading over a prolonged period of more than 1 year, when the solution containing these particles is stored under the dark and in ambient conditions. Our results also indicate that when deposited on a thin amorphous carbon film, the morphology and core–shell structure of the NRs remains unchanged after annealing to 120 °C in vacuum for several hours. The long-term stability of these core–shell NRs demonstrated here would be extremely useful when considering potential practical applications. Understanding the complex metal–metal interactions of this AuRh NR system offers possibilities for tuning the properties of these systems, with our study indicating potential to control the growth mode of Rh on Au NRs through influencing factors that drive the kinetics of Rh deposition. It may, in principle, be possible to alter the morphology of Rh deposition by using seeds of a different faceting structure to those used here, thus allowing for property tunability.

■ CONCLUSIONS

The present study demonstrates the successful deposition of Rh onto Au NRs via a sequential wet chemical route and the long-term stability of the resulting structure. We show that initial Rh deposition prefers the end and corner locations of Au NRs. The overall surface morphology of AuRh is uneven, where Rh tends to follow the island growth mode. We attribute the behavior of this system to energetic differences and large lattice strain between the constituent metals. This study of AuRh, an uncommon combination of two elements in a nanostructured system, yet potentially important in technological applications, furthers our understanding of the growth mechanism of Rh on Au NRs, revealing the potential, through better control of the

factors influencing the kinetics of Rh deposition during sample synthesis, to manipulate the morphology and chemical ordering of AuRh NRs and thus potentially tune their properties.

AUTHOR INFORMATION

Corresponding Author

*E-mail: z.li@bham.ac.uk (Z.Y.L.); s.l.horswell@bham.ac.uk (S.L.H.).

Notes

The authors declare no competing financial interest.

ACKNOWLEDGMENTS

We acknowledge financial support from the EPSRC (grant numbers: EP/D056241/1, EP/G070326/1) and the European Union through the FP7 Initial Training Network "ELCAT" (grant no. 214936-2) and the COST Action MP0903 "Nanoalloys as Advanced Materials: From Structure to Properties and Applications". R.L.C. and A.J.L. thank the EPSRC for studentships. The STEM instrument employed in this research was obtained through the Birmingham Science City project "Creating and Characterising Next Generation Advanced Materials", supported by AWM and ERDF.

REFERENCES

(1) Goesmann, H.; Feldmann, C. *Angew. Chem., Int. Ed.* **2010**, *49*, 1362−1395.
(2) Cuenya, B. R. *Thin Solid Films* **2010**, *518*, 3127−3150.
(3) Baletto, F.; Ferrando, R. *Rev. Mod. Phys.* **2005**, *77*, 371−423.
(4) Ferrando, R.; Jellinek, J.; Johnston, R. L. *Chem. Rev.* **2008**, *108*, 845−910.
(5) Herzing, A. A.; Kiely, C. J.; Carley, A. F.; Landon, P.; Hutchings, G. J. *Science* **2008**, *321*, 1331−1335.
(6) Kittel, C. *Introduction to Solid State Physics*; John Wiley & Sons: Hoboken, NJ, 2008.
(7) Kukovecz, A.; Potari, G.; Oszko, A.; Konya, Z.; Erdohelyi, A.; Kiss, J. *Surf. Sci.* **2011**, *605*, 1048−1055.
(8) Ovari, L.; Bugyi, L.; Majzik, Z.; Berko, A.; Kiss, J. *J. Phys. Chem. C* **2008**, *112*, 18011−18016.
(9) Essinger-Hileman, E. R.; DeCicco, D.; Bondi, J. F.; Schaak, R. E. *J. Mater. Chem.* **2011**, *21*, 11599−11604.
(10) Nikoobakht, B.; El-Sayed, M. A. *Chem. Mater.* **2003**, *15*, 1957−1962.
(11) He, W.; Wu, X.; Liu, J.; Zhang, K.; Chu, W.; Feng, L.; Hu, X.; Zhou, W.; Xie, S. *J. Phys. Chem. C* **2009**, *113*, 10505−10510.
(12) Liu, M.; Guyot-Sionnest, P. *J. Phys. Chem. B* **2005**, *109*, 22192−22200.
(13) Draine, B. T.; Flatau, P. J. *J. Opt. Soc. Am. A* **1994**, *11*, 1491−1499.
(14) Ferrer, D.; Torres-Castro, A.; Gao, X.; Sepulveda-Guzman, S.; Ortiz-Mendez, U.; Jose-Yacaman, M. *Nano Lett.* **2007**, *7*, 1701−1705.
(15) Wang, Z. W.; Li, Z. Y.; Park, S. J.; Abdela, A.; Tang, D.; Palmer, R. E. *Phys. Rev. B* **2011**, *84*, 073408.
(16) Li, Z. Y.; Yuan, J.; Chen, Y.; Palmer, R. E.; Wilcoxon, J. P. *Appl. Phys. Lett.* **2005**, *87*, 243103.
(17) Grzelczak, M.; Perez-Juste, J.; Rodriguez-Gonzalez, B.; Liz-Marzan, L. M. *J. Mater. Chem.* **2006**, *16*, 3946−3951.
(18) Kreibig, U.; Vollmer, M. *Optical Properties of Metal Clusters*; Springer: Berlin, Germany, 1995.
(19) Wang, Z. L.; Mohamed, M. B.; Link, S.; El-Sayed, M. A. *Surf. Sci.* **1999**, *440*, L809−L814.
(20) Katz-Boon, H.; Rossouw, C. J.; Weyland, M.; Funston, A. M.; Mulvaney, P.; Etheridge, J. *Nano Lett* **2011**, *11*, 273−278.
(21) Kibler, L. A.; Kleinert, M.; Kolb, D. M. *J. Electroanal. Chem.* **1999**, *467*, 249−257.
(22) Tenney, S. A.; Ratliff, J. S.; Roberts, C. C.; He, W.; Ammal, S. C.; Heyden, A.; Chen, D. A. *J. Phys. Chem. C* **2010**, *114*, 21652−21663.